Role of pressure in nonlinear velocity gradient dynamics in turbulence

Ravi K. Bikkani and Sharath S. Girimaji
Aerospace Engineering Department, Texas A & M University, College Station, Texas 77843, USA
(Received 3 October 2005; revised manuscript received 29 November 2006; published 16 March 2007)

To identify and understand the effect of pressure on turbulence velocity gradient dynamics, we study the velocity gradient evolution with the inviscid three-dimensional Burgers equation and the restricted Euler equation (REE). While the REE represents the incompressible limit of turbulence, the Burgers equation is taken to be the infinite Mach number model for the Navier-Stokes equation wherein the time scale of flow inertia is very small compared to that of pressure. Analytical fixed-point solutions for the velocity gradient tensor are obtained in the two cases. The results are compared and contrasted to isolate the role of pressure in shaping velocity gradient behavior. Of particular interest is the influence of pressure on (i) the strain rate eigenvalues; (ii) the sign of the intermediate principal strain rate; (iii) the tendency of vorticity to align with the intermediate principal strain rate; and (iv) the energy cascade direction. Importantly, the study provides valuable insight into the velocity gradient dynamics in highly compressible turbulence.

DOI: 10.1103/PhysRevE.75.036307 PACS number(s): 47.27.−i

I. INTRODUCTION

Velocity gradient dynamics hold the key to understanding many turbulence phenomena such as energy cascade, material element deformation, scalar mixing, and intermittency. The orientation between the vorticity vector and eigendirections of the strain-rate tensor is crucial as it determines whether vortices experience stretching or compression. The magnitude and sign of the strain-rate eigenvalues establish the nature of the self-straining of the velocity gradients. Vortex stretching and self-straining together dictate the direction of the energy cascade and the nature of intermittency. The orientation between the strain-rate eigendirections and scalar gradient controls the degree of isoscalar surface stretching, the scalar gradient magnification, and, ultimately, the efficiency of mixing. The velocity gradient dynamics depends upon the complex interplay between flow inertia, pressure, and viscous effects. The vortex stretching and self-straining physics is contained in the nonlinear inertia term, which is also responsible for wave-number proliferation or spectral broadening. Inertial effects cause velocity gradients to sharpen and at high enough Mach number shocks can form. The effect of pressure is to mitigate the material element straining and velocity gradient sharpening due to nonlinear inertia effects. At low Mach numbers, the restraining role of pressure is crucial for preserving the incompressibility condition. Viscous effects are manifest at high wave numbers and their role is quite straightforward: they draw kinetic energy from the flow and convert it into internal energy. On the other hand, the interplay between inertia and pressure effects is quite complicated and strongly dependent on the degree of compressibility. The main difference in the velocity gradient behavior between compressible and incompressible turbulence stems from the change in the role of pressure and the consequent modification of the pressure-inertia dynamic.

The objective of our work is to study the role of pressure in the velocity gradient behavior in turbulent flows. The Mach number characterizes the ratio of inertial to pressure effects in a flow. In incompressible (vanishingly small Mach number) flow, the time scale of pressure is much smaller than that of flow inertia. At the other extreme, in an infinite Mach number flow the time scale of pressure is very large compared to that of flow inertia. It is our plan to examine the velocity gradient behavior in these two extreme Mach number regimes to clearly establish the role of pressure. It is also reasonable to expect that this study will yield valuable insight into the velocity gradient behavior at intermediate Mach numbers.

Experimental examination of velocity gradient dynamics is possible only at low Reynolds numbers due to the high temporal and spatial resolution requirements. Computational studies that entail solving the full Navier-Stokes equations exactly at high Reynolds numbers will also be challenging for the same reasons. We will perform this investigation in inviscid flow, as viscous effects do not considerably modify the pressure-inertia interaction. We employ simple inviscid analytical and computational models that capture the essential features of the velocity gradient interactions in turbulence at the two limits. As these phenomena are nonlinear by their very nature, linear analyses such as rapid distortion theory (RDT) are not very useful. In this study, we analyze the behavior of velocity gradient dynamics in the inviscid Burgers and restricted Euler solutions. The restricted Euler equation is an excellent model of the velocity gradient dynamics in incompressible turbulence. In inviscid Burgers turbulence, which is also called pressure-released turbulence, only the inertial effects are considered and this represents a reasonable model of Navier-Stokes turbulence in the infinite Mach number limit.

Restricted Euler equation. Viellefosse [1] was the first to study velocity gradient evolution in incompressible turbulence using a simple autonomous dynamical system of equations called the restricted Euler equations (REEs). These equations are obtained by neglecting the anisotropic pressure Hessian ($H_{ij}=0$) in the Euler velocity gradient equations. Viellefosse [1] also performed approximate but important asymptotic analysis of restricted Euler equation. Ashurst and Kerstien [2] demonstrated that the REE accurately captures many of the strain-rate and vorticity characteristics observed in direct numerical simulations (DNSs) of isotropic and ho-

mogeneous shear incompressible turbulence: (i) the strain-rate tensor exhibits two positive and one negative eigenvalues; (ii) the magnitude of the intermediate eigenvalue is much smaller than that of the others; and (iii) vorticity is aligned with the intermediate eigenvector. Cantwell [3] developed more detailed solutions of the restricted Euler equation and compared the results with isotropic DNS data. Invariant maps which facilitate the study of velocity gradient geometry were introduced in this work. Girimaji and Speziale [4] developed the modified restricted Euler equation that can be used for flows with nonzero mean velocity gradient. Three different strategies for modeling the viscous effects have been proposed in the literature. Girimaji and Pope [5] account for viscous effects using a stochastic diffusion model. Chertkov *et al.* [6] propose a model based on Lagrangian tetrad dynamics. Jeong and Girimaji [7] perform a Lagrangian material deformation analysis and propose a variable-time-scale viscous relaxation model. Most recently, Chevillard *et al.* [8] have significantly enhanced the REE well beyond its original intent and scope. In a series of articles they demonstrate that the enhanced REE can accurately describe the physics of intermittency and predict scaling exponents of structure functions. In summary, for elementary modeling of many nonlinear velocity gradient interactions, the incompressible REE is quickly becoming what RDT is to linear turbulence processes.

Burgers equation. There have been numerous studies of Burgers turbulence, or pressure-released turbulence, in the literature which examine its relation to Navier-Stokes turbulence. Many aspects of the nonlinear turbulence cascade in highly compressible flows are well captured by the Burgers equation. For example, the probability density functions (PDFs) of velocity and velocity gradients obtained from the Burgers equations share similarities with those from Navier-Stokes equations [9,10]. The connection between the Burgers equation and the Navier-Stokes equation at very high Mach numbers is also discussed in [11]. Girimaji and Zhou [12] demonstrate that the triadic interactions in the one-dimensional (1D) Burgers equation are quite similar to those in 3D Navier-Stokes turbulence. Thus, despite its simplicity, the Burgers equation can offer crucial insight into compressible turbulence physics.

In this study, exact fixed-point solutions of both the Burgers and the restricted Euler equations are derived. It is demonstrated that the parametric solution obtained in [3] is one of the three fixed points of the REE. Numerical computations are then performed to isolate the stable solutions from the complete set of fixed points. The stable solutions are then further investigated for highlighting fixed-point flow physics. In particular, we are interested in the three main features: (i) the sign of intermediate principal strain-rate tensor, (ii) the alignment of vorticity, and (iii) the direction and rate of energy cascade. The results from the two sets of equations are compared to isolate the effect of pressure.

The governing velocity gradient equations for Burgers turbulence and restricted Euler equations are derived in Sec. II. In Sec. III, the fixed-point solutions are obtained and their properties are discussed. Finally, we present a brief summary of our findings in Sec. IV.

II. GOVERNING EQUATIONS

We first derive the velocity gradient evolution equation in 3D Burgers turbulence. The evolution equations for strain-rate tensor and rotation tensor are then obtained. Finally we present a brief derivation of the restricted Euler equation for normalized velocity gradients.

A. Burgers equation

The inviscid 3D Burgers equation, given by

$$\frac{\partial u_i}{\partial t} + u_k \frac{\partial u_i}{\partial x_k} = 0, \tag{1}$$

is differentiated with respect to x_j, leading to

$$\frac{\partial A_{ij}}{\partial t} + u_k \frac{\partial A_{ij}}{\partial x_k} + A_{ik}A_{kj} = 0 \quad \text{or} \quad \frac{dA_{ij}}{dt} + A_{ik}A_{kj} = 0. \tag{2}$$

where A_{ij} is the velocity gradient tensor, $A_{ij} = \partial u_i / \partial x_j$, and d/dt represents the Lagrangian derivative. The incompressibility condition is not satisfied as the Burgers equation does not include the pressure term. As viscous effects are also neglected, the evolution equation for A_{ij} may diverge in finite time and therefore these equations are not suitable for numerical computations or fixed-point analysis. In order to overcome this problem, a normalized velocity gradient tensor (b_{ij}) is defined [7],

$$b_{ij} = \frac{A_{ij}}{\sqrt{\varepsilon}} \quad \text{where } \varepsilon = A_{mn}A_{mn}. \tag{3}$$

The b_{ij} tensor contains all the geometric information of the velocity gradient tensor (A_{ij}) and is better suited for numerical computations. The evolution equation of b_{ij} can now be obtained from Eq. (2),

$$\frac{\partial b_{ij}}{\partial t} = -\sqrt{\varepsilon}(b_{ik}b_{kj} - b_{ij}b_{mn}b_{mk}b_{kn}). \tag{4}$$

This equation still contains $\sqrt{\varepsilon}$, which may diverge in finite time. Since we are interested in the asymptotic behavior of the velocity gradient tensor such a divergence is not desirable. Therefore the evolution of b_{ij} is studied in normalized time,

$$\partial t' = \sqrt{\varepsilon}\partial t. \tag{5}$$

Equation (4) can now be rewritten as

$$\frac{\partial b_{ij}}{\partial t'} = -(b_{ik}b_{kj} - b_{ij}b_{mn}b_{mk}b_{kn}). \tag{6}$$

This is a simple first-order ordinary differential equation (ODE) system that can be solved numerically for b_{ij} given the initial condition. As we are interested in the behavior of the strain-rate tensor and the vorticity, the velocity gradient tensor is decomposed into its symmetric part (strain-rate tensor s_{ij}) and its antisymmetric part (rotation tensor w_{ij}). Equation (6) can now be used to obtain separate evolution equations for s_{ij} and w_{ij}:

$$\frac{\partial s_{ij}}{\partial t'} = s_{ij}(b_{mn}b_{mk}b_{kn}) - s_{ik}s_{kj} - w_{ik}w_{kj}, \tag{7}$$

$$\frac{\partial w_{ij}}{\partial t'} = w_{ij}(b_{mn}b_{mk}b_{kn}) - s_{ik}w_{kj} - w_{ik}s_{kj}. \quad (8)$$

Equations (7) and (8) constitute an autonomous system of ODEs which dictate the velocity gradient dynamics of Burgers turbulence. Exact solutions of these equations cannot be obtained easily. However, important physical aspects of this system of equations can be extracted from a fixed-point analysis. This analysis will be performed in the next section.

B. Restricted Euler equation

The Euler equation for velocity gradients can be written as [3]

$$\frac{dA_{ij}}{dt} + A_{ik}A_{kj} - A_{mk}A_{km}\frac{\delta_{ij}}{3} = H_{ij} \quad (9)$$

where $H_{ij} = -[\partial^2 p/\partial x_i \partial x_j - (\partial^2 p/\partial x_k \partial x_k)\delta_{ij}/3]$.

In this work, we follow the precedent of Vieillefosse [1], Cantwell [3], and Girimaji *et al.* [5] and neglect the pressure Hessian ($H_{ij}=0$) leading to the restricted Euler equations. Normalization of the velocity gradients and scaling of time as done with the Burgers equations leads to

$$\frac{\partial b_{ij}}{\partial t'} = -\left(b_{ik}b_{kj} - \frac{1}{3}(b_{mk}b_{kn})\delta_{ij} - b_{ij}b_{mn}b_{mk}b_{kn}\right). \quad (10)$$

The corresponding evolution equations for s_{ij} and w_{ij} are given by

$$\frac{\partial s_{ij}}{\partial t'} = s_{ij}(b_{mn}b_{mk}b_{kn}) + \frac{1}{3}(b_{mk}b_{kn})\delta_{ij} - s_{ik}s_{kj} - w_{ik}w_{kj}, \quad (11)$$

$$\frac{\partial w_{ij}}{\partial t'} = w_{ij}(b_{mn}b_{mk}b_{kn}) - s_{ik}w_{kj} - w_{ik}s_{kj}. \quad (12)$$

Equations (11) and (12) dictate the velocity gradient evolution in restricted Euler turbulence.

Equations (7), (8), (11), and (12) are investigated to obtain a better understanding of the role of pressure in the velocity gradient dynamics in turbulent flows. The behavior of velocity gradients is studied in terms of its invariants as proposed by Cantwell [3]. The various velocity gradient invariants are

$$P(t') = -b_{ii}, \quad Q(t') = -\frac{1}{2}b_{im}b_{mi}, \quad (13)$$

and

$$R(t') = -\frac{1}{3}b_{im}b_{mk}b_{ki}.$$

Each of these invariants has a specific physical significance in the context of turbulent flows. $P(t')$ is the dilatation (with a negative sign) of the velocity field. Negative $P(t')$ (positive dilatation) implies that the fluid element is expanding and positive $P(t')$ means that the fluid element is contracting. The fact that incompressibility is satisfied in case of the restricted Euler equations means that $P(t')=0$, a condition which is not necessarily satisfied with the Burgers equation set. $Q(t')$ represents the difference between the magnitude of strain and vorticity. If $Q(t')$ is positive, then the magnitude of rotation exceeds that of strain and vice versa. $R(t')$ is an indicator of the energy cascade rate as will be seen later.

III. RESULTS AND DISCUSSION

The unnormalized velocity gradient REE has been subject to parametric analysis in previous work [3]. In this study we adopt a slightly different approach. Rather than examine the time evolution of the velocity gradients, we focus on its equilibrium or fixed-point behavior. The fixed-point behavior is independent of the initial conditions and, more importantly, it reveals the inherent physics incumbent in the system of equations. In the absence of any external influences, the system state variables will asymptote to the stable fixed-point values. Saddle fixed points can dictate the behavior of the system for short periods of time. Hence, fixed-point and accompanying stability analysis can provide important insight into the physics of the system. Here, we first obtain fixed-point solutions of the two systems analytically. Since the governing equations are quite complicated, a formal stability analysis of the fixed points is not feasible. Instead, we identify the stable fixed points using numerical simulations. Then, the velocity gradient dynamics is investigated in detail at the stable fixed points. The results from Burgers equations are then compared with the restricted Euler results to identify the effect of pressure. The difference between the two solutions will also reflect the difference between velocity gradient physics in incompressible and compressible flows.

A. Fixed-point analysis of the restricted Euler equation

The fixed-point equations are obtained from Eqs. (11) and (12) by setting the time derivative to zero:

$$s_{ij}(b_{mn}b_{mk}b_{kn}) + \frac{1}{3}(b_{mk}b_{kn})\delta_{ij} - s_{ik}s_{kj} - w_{ik}w_{kj} = 0,$$

$$w_{ij}(b_{mn}b_{mk}b_{kn}) - s_{ik}w_{kj} - w_{ik}s_{kj} = 0. \quad (14)$$

The fixed points are the roots of the above equations which can be rewritten as

$$s_{ij} = \frac{s_{ik}s_{kj} - w_{ik}w_{kj} - \frac{1}{3}(b_{mk}b_{kn})\delta_{ij}}{b_{mn}b_{mk}b_{kn}} \quad \text{for } i,j = 1,2,3.$$

$$w_{ij} = \frac{w_{ik}s_{kj} - w_{ik}s_{kj}}{b_{mn}b_{mk}b_{kn}}. \quad (15)$$

These solutions need further investigation. Without loss of generality, we can assume that the coordinate axes of the reference frame are aligned with the principal strain-rate tensor in the asymptotic limit. Hence s_{ij} and w_{ij} tensors are of the form

$$s_{ij} = \begin{vmatrix} s_{11} & 0 & 0 \\ 0 & s_{22} & 0 \\ 0 & 0 & s_{33} \end{vmatrix} \quad \text{and} \quad w_{ij} = \begin{vmatrix} 0 & w_{12} & w_{13} \\ -w_{12} & 0 & w_{23} \\ -w_{13} & -w_{23} & 0 \end{vmatrix}. \tag{16}$$

In other words, (s_{11}, s_{22}, s_{33}) are the eigenvalues of the strain-rate tensor. We also arrange the solutions such that $s_{11} \geqslant s_{22} \geqslant s_{33}$. We can then simplify Eq. (15) to a set of six equations with six unknowns. These equations are additionally subject to the constraint that the norm of b_{ij} tensor be equal to unity by definition:

$$s_{11}^2 + s_{22}^2 + s_{33}^2 + 2(w_{12}^2 + w_{13}^2 + w_{23}^2) = 1. \tag{17}$$

The incompressibility condition is automatically satisfied by the fixed-point solution. These nonlinear set of equations are solved analytically in MATHCAD. Three sets of fixed-points are identified for this system of nonlinear equations as follows.

Set 1

$$(s_{11}, s_{22}, s_{33}) = (0,0,0) \quad \text{and} \quad w_{12} = \pm\frac{1}{\sqrt{6}}, \quad w_{13} = \pm\frac{1}{\sqrt{6}}, \quad w_{23} = \pm\frac{1}{\sqrt{6}} \quad \text{(all eight different possible combinations)}. \tag{18}$$

Set 2

$$(s_{11}, s_{22}, s_{33}, w_{12}, w_{13}, w_{23}) = \left(\sqrt{-\frac{2}{3}w_{13}^2 + \frac{5}{12} + y}, -\frac{1}{3}\frac{\left(-w_{13}^2 + \frac{1}{4} + 3y\right)}{\sqrt{-\frac{2}{3}w_{13}^2 + \frac{5}{12} + y}}, \frac{1}{3}\frac{(w_{13}^2 - 1)}{\sqrt{-\frac{2}{3}w_{13}^2 + \frac{5}{12} + y}}, 0, w_{13}, 0 \right).$$

Set 3

$$(s_{11}, s_{22}, s_{33}, w_{12}, w_{13}, w_{23}) = \left(\sqrt{-\frac{2}{3}w_{13}^2 + \frac{5}{12} - y}, -\frac{1}{3}\frac{\left(-w_{13}^2 + \frac{1}{4} - 3y\right)}{\sqrt{-\frac{2}{3}w_{13}^2 + \frac{5}{12} - y}}, \frac{1}{3}\frac{(w_{13}^2 - 1)}{\sqrt{-\frac{2}{3}w_{13}^2 + \frac{5}{12} - y}}, 0, w_{13}, 0 \right),$$

where $y = \frac{1}{12}\sqrt{48w_{13}^4 - 48 \cdot w_{13}^2 + 9}$.

Set 1 has no free parameters. Sets 2 and 3 represent a family of fixed points parametrized by w_{13}.

To identify the stable solutions, Eq. (10) is solved numerically using the fourth-order Runge-Kutta method. We randomly generate 2000 different initial velocity gradient tensors $[b_{ij}(t'=0)]$ and solve the velocity gradient equations to obtain the asymptotic solutions. These results are studied in terms of the invariants of the b_{ij} tensor (Q vs R). In the case of restricted Euler equations, a parametric equation can be obtained that relates the invariants (Q,R) [3],

$$R = \pm\left(-\frac{4}{27}Q^3\right)^{1/2}. \tag{19}$$

It can be shown that Eq. (19) corresponds to the fixed-point family represented by set 3. Thus, the parametric solution obtained in [3] is one of the fixed points of the REE. Clearly, the present fixed-point study provides a more complete analysis than [3] by identifying other behavior permitted by the REE.

Figure 1 shows the invariant behavior obtained from numerical computations of the REE. Each point corresponds to the asymptotic state reached from a random initial condition. As expected, all the points lie on the trajectory prescribed by Eq. (19) or set 3. Therefore, the stable fixed point is a family

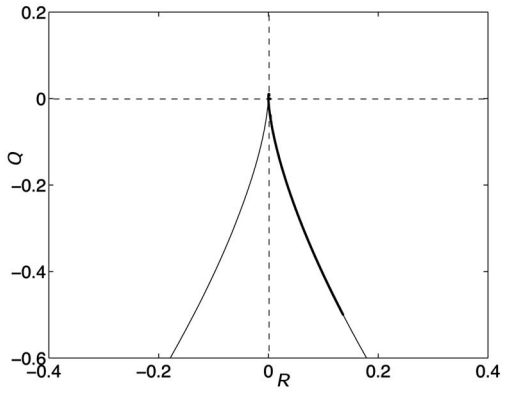

FIG. 1. Invariant plot from computations of restricted Euler equation. Thin solid line, Eq. (19); bold line, restricted Euler computations.

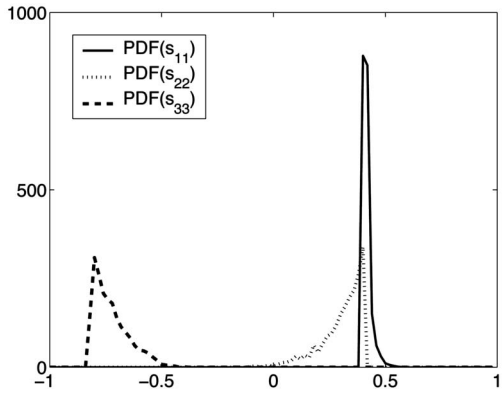

FIG. 2. PDF of asymptotic principal strain rates from computations of restricted Euler equations.

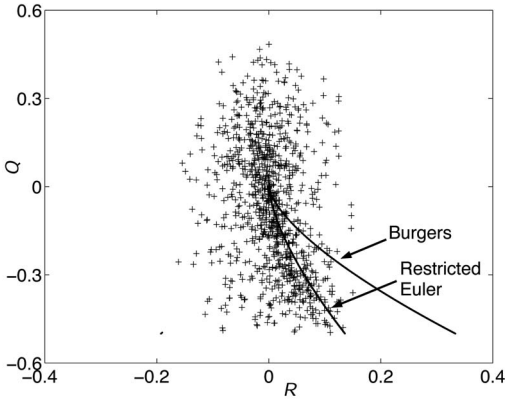

FIG. 3. DNS results of decaying isotropic turbulence. +, DNS results.

of solutions represented by set 3 with one free parameter (w_{13}). We investigate further the properties of the stable solution—set 3.

Strain-rate tensor. Figure 2 shows the PDF of principal strain rates from numerical computations. We can clearly see that the intermediate strain rate s_{22} is positive and its magnitude is small compared to those of the other two strain rates.

Vorticity vector. The vorticity vector ($\vec{\omega}$) is related to the rotation tensor (w_{ij}) by the Levi-Cività tensor (e_{ijk})

$$\omega_k = \frac{1}{2} e_{ijk} w_{ij}. \tag{20}$$

Using this relation, the vorticity vector corresponding to the stable fixed point is calculated,

$$(\omega_1, \omega_2, \omega_3) = (0, -w_{13}, 0). \tag{21}$$

It can be seen that the vorticity vector has only one component (ω_2) and it is indeed aligned with the intermediate strain rate (s_{22}).

Energy cascade. The energy cascade can be studied in terms of the rate of change of magnitude of the velocity gradient tensor (ε). Increase in the magnitude of ε corresponds to gradient steepening. Gradient steepening or sharpening implies that the length scale associated with a fluid particle (containing a certain amount of energy) decreases. Therefore, gradient steepening indicates forward energy cascade. Decrease in the value of ε, on the other hand, implies gradient smoothing or an inverse energy cascade. Thus, a positive rate of change of ε is an indication that energy is being transferred from large scales to small scales, and a negative rate of change indicates the inverse transfer.

The evolution of ε can be obtained using Eq. (9),

$$\frac{d\varepsilon}{dt} = -2A_{mk}A_{kn}A_{mn}. \tag{22}$$

Decomposing A_{ij} into its symmetric and antisymmetric parts and using the form defined by Eq. (16) for s_{ij} and w_{ij}, the right-hand side of Eq. (22) can be rewritten as

$$\frac{d\varepsilon}{dt'} = -2\varepsilon[s_{11}(s_{11}^2 + w_{12}^2 + w_{13}^2) + s_{22}(s_{22}^2 + w_{12}^2 + w_{23}^2) + s_{33}(s_{33}^2 + w_{13}^2 + w_{23}^2)]. \tag{23}$$

In the above equation, terms on the right-hand side (RHS) of the form *sss* represent self-straining and those of the form *sww* correspond to vortex stretching or compression. Upon substituting the stable solution values of various components and simplifying, we get

$$\frac{d\varepsilon}{dt'} = 2\varepsilon(s_{22}). \tag{24}$$

Since it is already shown that s_{22} is non-negative, the right-hand side of Eq. (24) is non-negative. Thus, at the asymptotic state, the energy transfer in incompressible flows can only be from large to small scales. Inverse transfer may be possible in transient states. Closer examination of the individual terms in Eq. (23) will reveal that both vortex stretching and self-straining contribute to forward cascading of energy.

In summary, we have been able to demonstrate (i) previously known [2,3] trends and results analytically; and (ii) a strong tendency for a forward energy cascade in incompressible turbulence. Next, we compare the numerical computations of restricted Euler equations with direct numerical simulation of decaying isotropic and homogeneous anisotropic velocity fields. The decaying isotropic DNS data are obtained from [13] and the homogeneous anisotropic DNS data from [14]. Figures 3 and 4 show the DNS results of decaying isotropic and decaying homogeneous anisotropic velocity fields, respectively. It is to be noted that the invariants in DNS scatter plots are calculated from the normalized velocity gradients and these variables are different from those used in [3]. Clearly, the agreement between the REE stable normalized fixed-point solution (set 3) and DNS is quite good.

B. Fixed-point analysis of the Burgers equation

The Burgers fixed-point equations are

$$s_{ij}(b_{mn}b_{mk}b_{kn}) - s_{ik}s_{kj} - w_{ik}w_{kj} = 0,$$

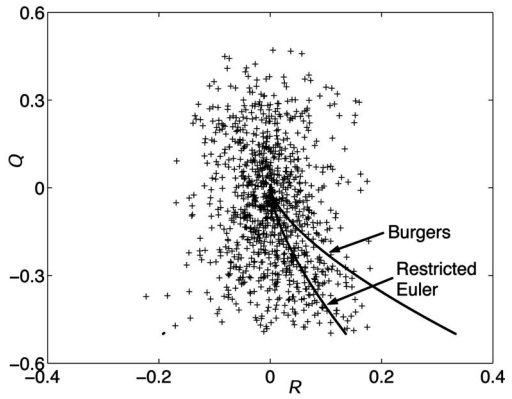

FIG. 4. DNS results of decaying homogeneous anisotropic turbulence. +, DNS results.

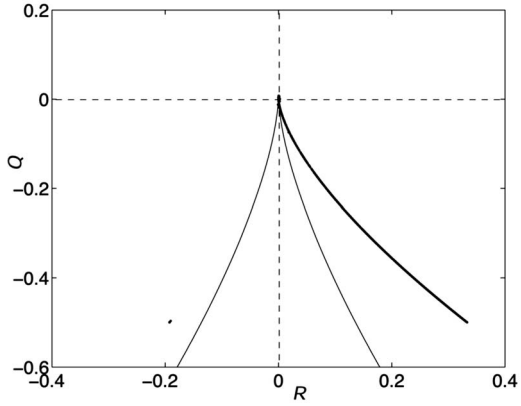

FIG. 5. Invariant plot from computations of Burgers equations. Thin solid line, Eq. (6); bold line, from Burgers computations.

$$w_{ij}(b_{mn}b_{mk}b_{kn}) - s_{ik}w_{kj} - w_{ik}s_{kj} = 0. \tag{25}$$

From the above, implicit equations for strain rate and rotation can be easily derived:

$$s_{ij} = \frac{s_{ik}s_{kj} - w_{ik}w_{kj}}{b_{mn}b_{mk}b_{kn}} \quad \text{and} \quad w_{ij} = \frac{w_{ik}s_{kj} - w_{ik}s_{kj}}{b_{mn}b_{mk}b_{kn}}$$

$$\text{for } i,j = 1,2,3. \tag{26}$$

Again, these equations are subject to the constraint that the norm of the b_{ij} tensor equals unity [Eq. (17)]. Solving these equations for principal rates of strain and rotation tensors we get four sets of fixed-point solutions.

Set 1

$$(s_{11},s_{22},s_{33},w_{12},w_{13},w_{23}) = \left(-\frac{1}{\sqrt{3}},-\frac{1}{\sqrt{3}},-\frac{1}{\sqrt{3}},0,0,0\right). \tag{27}$$

Set 2

$$(s_{11},s_{22},s_{33},w_{12},w_{13},w_{23}) = \left(\frac{1}{\sqrt{3}},\frac{1}{\sqrt{3}},\frac{1}{\sqrt{3}},0,0,0\right).$$

Set 3

$$(s_{11},s_{22},s_{33},w_{12},w_{13},w_{23}) = (s_{11},0,s_{11}-1,0,\pm\sqrt{s_{11}-s_{11}^2},0).$$

Set 4

$$(s_{11},s_{22},s_{33},w_{12},w_{13},w_{23}) = (s_{11},-z+s_{11},-z,0,\pm\sqrt{s_{11}z},0).$$

Here $z=\frac{1}{2}\sqrt{2-4s_{11}^2}$.

Sets 3 and 4 are characterized by a single free parameter s_{11}. These solutions constitute the entire possible fixed-point solution set—both stable and unstable solutions. Note that the incompressibility condition is not satisfied by these solutions ($\Sigma s_{ii} \neq 0$) due to the absence of pressure in this high Mach number model.

Numerical computations of Eq. (6) are performed using the fourth-order Runge-Kutta method. Once again 2000 Lagrangian particles with randomly generated initial velocity gradient tensors $[b_{ij}(t'=0)]$ are used in the computations. Figure 5 shows the Q vs R plot for the Burgers velocity gradient equations. From the numerical results, we find that fixed-point sets 2 and 3 are both stable. Set 2 corresponds to the single fixed point as seen in the third quadrant of Fig. 5 and set 3 corresponds to the family of solutions in the fourth quadrant. It is observed from the numerical results that nearly 30% of the trajectories are attracted to set 2 and the remainder to set 3. Hence we can say that set 2 is the minor attractor and set 3 is the major attractor. Let us now examine the physics of the two stable sets.

Dilatation. Upon relaxation of the incompressibility constraint, it will be interesting to observe if the fluid elements tend to expand, contract, or preserve their initial volume. To answer this question, we must inspect the behavior of the first invariant of the velocity gradient tensor, P. We note that $P(t')$ is negative for set 2, implying that the fluid elements evolving according to this fixed-point physics experience expansion. As the three velocity gradient eigenvalues are identical, we can further observe that the expansion is spherically isotropic. On the other hand, $P(t')$ is positive for set 3, indicating that these fluid elements are contracting. When s_{11} is zero, the fixed-point solution is a one-dimensional compression wave or shock.

Strain-rate tensor. In the case of the major attractor (set 3) the intermediate principal strain rate is zero as opposed to being positive as observed in the case of restricted Euler solutions. On the other hand, all the particles attracted to set 2 experience a uniform positive strain in all directions.

Vorticity vector. The vorticity vectors corresponding to the stable fixed-point sets 2 and 3 are

$$(\omega_1,\omega_2,\omega_3) = (0,0,0) \quad \text{(set 2)},$$

$$(\omega_1,\omega_2,\omega_3) = (0,\mp\sqrt{s_{11}-s_{11}^2},0) \quad \text{(set 3)}. \tag{28}$$

It can be seen that in the case of set 3 ω_2 is the only nonzero component. Hence the vorticity vector is aligned with the intermediate strain rate (s_{22}), which is zero. In the case of set 2, the vorticity is zero and the velocity field experiences pure strain. This clearly indicates that vortex stretching may not be important in high Mach number turbulence.

Energy transfer. Energy transfer is studied further in terms of the rate of change of ε as was done earlier with

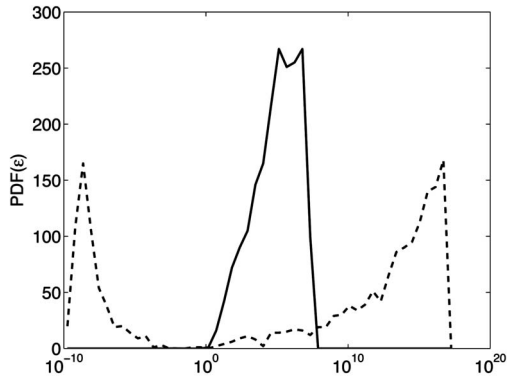

FIG. 6. PDF of magnitude of velocity gradient tensor (ε) in the asymptotic limit. Solid line, restricted Euler results; dashed line, Burgers results.

restricted Euler equations. The equation for ε is of the same form for both restricted Euler and Burgers equations. Hence, using Eq. (22), the evolution equations for ε corresponding to each stable set are

$$\frac{d\varepsilon}{dt'} = -\frac{\varepsilon}{\sqrt{3}} \quad \text{(set 2)},$$

$$\frac{d\varepsilon}{dt'} = \varepsilon(1 - 2s_{11}) \quad \text{(set 3)}. \tag{29}$$

The right-hand side, in the case of set 3, is always positive as the numerical computations indicate that all the points belonging to the fixed-point set 3 are such that $s_{11} \leqslant 0.5$. Hence, in this case we have positive growth of velocity gradients, which implies a forward energy cascade as expected. With set 2, the right-hand side is negative, indicating that energy is transferred from small scales to large scales, i.e., an inverse energy cascade. This is consistent with the numerical computations (Fig. 5): $R(t')$ is negative for set 2, indicating an inverse energy cascade, whereas R is positive for set 3, implying a forward cascade. It is important to note that all of the cascading is due to self-straining and vortex stretching is completely absent at these fixed points.

We next examine the magnitude of velocity gradients (ε) at the asymptotic limit in the two cases to better highlight the differences in energy transfer. As mentioned before, a large magnitude of ε implies rapid forward energy transfer and very low magnitudes imply gradient smoothening or inverse energy transfer. Figure 6 shows the PDF of the asymptotic ε's from both Burgers and restricted Euler computations. In the case of the Burgers results, we have two distinctly concentrated regions—one at very high magnitudes and the other at low magnitudes. From the numerical computations, it is found that all the low-magnitude ε's correspond to set 2 whereas the high-magnitude ε's correspond to set 3. The restricted Euler ε's are concentrated in the intermediate range. Thus the dissipation probability distribution function will have heavier and longer tails in compressible turbulence, indicating a greater degree of intermittency than in incompressible turbulence.

C. Effect of pressure

As mentioned in the Introduction, one of the principal differences in velocity gradient dynamics between incompressible and compressible turbulence originates from the difference in the role of pressure in the two cases. Clearly, the most fundamental role of pressure is to uphold the incompressibility condition. In the absence of pressure, fluid particles may expand or contract depending upon the initial condition. The expanding particles experience spherically symmetric dilation, and vorticity, if present initially, is suppressed by the time the asymptotic state is reached. Further, the velocity gradients associated with these particles decrease, indicating transfer of energy from small to large scales. Contracting particles exhibit a completely different behavior: the velocity gradients increase in magnitude, indicating forward transfer of energy. Although vorticity is nonzero, there is insignificant vortex stretching in the asymptotic state. In fact, the bimodal behavior observed in the Burgers equation calculations—simultaneous direct and inverse energy cascades—has been seen in earlier studies of compressible turbulence and magnetohydrodynamic turbulence [15–18].

It is not unreasonable to expect that the velocity gradient dynamics in finite Mach number turbulence will fall between the REE and Burgers behavior. At high Mach numbers, as the pressure effects are gradually introduced into Burgers turbulence, it is likely that the forward cascade rate of expanding particles will diminish and the inverse transfer tendencies of contracting particles will be negated. When the pressure effects are strong enough (low Mach numbers), it is likely that the REE behavior will be more prominent. Our study also implies that much of the dissipation will occur in high-strain regions of the flow in high Mach number turbulence, in contrast to high-vorticity regions in incompressible turbulence. This is due to the fact that vortex stretching is weaker at higher Mach numbers. These implications are very much in line with observations in compressible turbulence simulations.

IV. SUMMARY

We perform fixed-point and stability analysis of the Burgers and restricted Euler equations to examine the role of pressure in velocity gradient dynamics. These two equations are reasonable models for velocity gradients in the extreme limits of Mach number—the Burgers at the infinite pressure-released limit and the REE at the incompressible end. Comparison of the invariants of the velocity gradient tensor obtained from the Burgers and restricted Euler equations show the fundamental differences in turbulence cascade and other small-scale mechanisms between the two limiting cases. Analytical solutions of the restricted Euler equations are used to reaffirm some of the previous findings concerning the geometry of the velocity gradient tensor: (i) the intermediate principal strain rate is positive and smaller in magnitude compared to the other two strain rates; (ii) vorticity is aligned with the intermediate strain rate; and (iii) only a forward energy cascade is permissible and both vortex stretching and self-straining contribute toward the transfer. A simi-

lar analysis of Burgers asymptotic solutions leads to the following observations in the absence of pressure: (i) vortex stretching is inhibited, (ii) contracting fluid elements (which constitute about 70% of the samples considered) experience forward energy transfer at rates higher than comparable incompressible flow; (iii) expanding fluid elements (about 30% of the samples) undergo inverse energy transfer; (iv) self-straining is the leading cascade mechanism; and (v) the degree of intermittency may be higher than in incompressible flow. The bimodality observed in our analytical and numerical computations of Burgers turbulence is consistent with earlier studies of compressible turbulence [15–18].

This work was supported by AFOSR-MURI project.

[1] P. Vieillefosse, J. Phys. (Paris) **43**, 837 (1982).
[2] W. T. Ashurst and A. Kerstien, Phys. Fluids **30**, 2343 (1987).
[3] B. J. Cantwell, Phys. Fluids A **4**, 782 (1992).
[4] S. S. Girimaji and C. G. Speziale, Phys. Fluids **7**, 1438 (1995).
[5] S. S. Girimaji and S. B. Pope, Phys. Fluids A **2**, 242 (1990).
[6] M. Chertkov, A. Pumir, and B. I. Shraiman, Phys. Fluids **11**, 2394 (1999).
[7] E. Jeong and S. S. Girimaji, Theor. Comput. Fluid Dyn. **16**, 421 (2003). See also J. Martin *et al.*, Phys. Fluids **9**, 814 (1997).
[8] L. Chevillard and C. Meneveau, Phys. Rev. Lett. **97**, 174501 (2006).
[9] J.-P. Bouchaud and M. Mezard, Phys. Fluids **7**, 1438 (1995).
[10] M. Avellaneda, R. Ryan, and E. Weinan, Phys. Fluids **7**, 3067 (1995).
[11] T. Passot and E. Vázquez-Semadeni, Phys. Rev. E **58**, 4501 (1998).
[12] S. S. Girimaji and Y. Zhou, Phys. Lett. A **202**, 279 (1995); see also V. Borue and S. A. Orszag, J. Fluid Mech. **366**, 1 (1998).
[13] H. Yu, S. S. Girimaji, and L.-S. Luo, Phys. Rev. E **71**, 016708 (2005).
[14] D. Yu, J. Turbul. **6**, 1 (2005).
[15] G. Y. Antar, Phys. Rev. Lett. **91**, 055002 (2003).
[16] M. Chertkov, I. Kolokolov, and M. Vergassola, Phys. Rev. Lett. **80**, 512 (1998).
[17] M. Christensson, M. Hindmarsh, and A. Brandenburg, Phys. Rev. E **64**, 056405 (2001).
[18] M. A. Rutgers, Phys. Rev. Lett. **81**, 2244 (1998).